Local lattice distortions and electronic orders in strongly correlated systems by resonant total x-ray scattering: A case study of APt_2X_2 intermetallics (A = U, Ce, or La and X = Si or Ge)

V. Petkov [1,*] R. Baumbach,[2] M. Jakhar [1] V. Barone [1] A. Zafar [1] L. Gallington [3] S. Shastri,[3] and B. Aoun [4]

[1]*Department of Physics, Central Michigan University, Mount Pleasant, Michigan 48858, USA*

[2]*National High Magnetic Field Laboratory, Florida State University, Tallahassee, Florida 32310, USA*

[3]*X-Ray Science Division, Advanced Photon Source, Argonne National Laboratory, Argonne,Illinois 60439, USA*

[4]*fullrmc LLC, Dallas, Texas 75002, USA*

(Received 4 September 2023; accepted 21 November 2023; published 14 December 2023)

Revealing local lattice distortions in physical systems is nontrivial, largely because such structural features often are not necessarily amenable to traditional crystallographic investigations. This poses limits to our understanding of the underlying physics, particularly in the case of strongly correlated systems where structural, electronic, and magnetic degrees of freedom are intertwined. Using resonant total x-ray scattering coupled to differential pair distribution function analysis, we reveal the presence of pronounced local lattice distortions in the square net Pt planes in the prototypical strongly correlated APt_2X_2 intermetallics (A = U, Ce, or La and X = Si or Ge). The distortions are present before charge density wave, magnetic, Kondo lattice coherence, and/or superconducting orders emerge in these materials and, as density functional calculations suggest, are likely to affect them. Our study sheds light on the poorly known interactions between electronic orders and structural disorder in strongly correlated systems. It also demonstrates an advanced experimental approach to determine them that is relevant to any physical system showing deviations from perfect crystallinity.

DOI: 10.1103/PhysRevB.108.224110

I. INTRODUCTION

Competing interactions in strongly correlated systems are known to lead to the emergence of collectively ordered electronic states such as unconventional superconductivity (SC), charge density waves (CDWs), complex magnetic order, nematic order, and Kondo lattice coherence [1–12], to name a few. The orders appear intertwined in intricate phase diagrams [13–29] and are often coupled to lattice degrees of freedom, including local lattice distortions. Local lattice distortions are, however, nontrivial to reveal using traditional crystallographic techniques, rendering it difficult to assess their effect on the emerging electronic orders. Here we show that the problem may be addressed by using resonant total x-ray scattering coupled to differential pair distribution function (PDF) analysis. We apply the technique to five "122-type" APt_2X_2 intermetallics (A = U, Ce, or La, and X = Si or Ge) with the $CaBe_2Ge_2$ variant of the $ThCr_2Si_2$-type structure, where A atoms are located between $\{Pt_2X_2\}$ layers featuring square planes of Pt atoms. This structure is known as the "perovskite" of intermetallics and is adopted by many strongly correlated systems, including the topical 122-type AT_2Pn_2 pnictide superconductors (A = alkaline or rare earth, T = transition metal, and Pn = As, Sb, or P) [30–38]. The Pt-based analogs exhibit a variety of electronic orders and similar lattice distortions, allowing us to study their relationship on a common structural basis. In particular, they all exhibit CDW order involving the Pt species [21,30–33]. In addition, those containing f-electron free La species are SCs while the ones containing Ce and U species, which have partially filled f-electron shells, exhibit Kondo lattice phenomena [30]. Furthermore, UPt_2Si_2 develops antiferromagnetic order at low temperature [34,35]. We find that the intermetallics exhibit local lattice distortions that are manifested as a displacement of half of the Pt atoms from their position in the undistorted crystal lattice. The displacement exists at room temperature, i.e., well above the temperature of the emergence of collective CDW order at T_{CDW}, Kondo lattice coherence at T_{KL}, superconductivity at T_{SC}, and/or antiferromagnetic (AFM) order at T_N in the respective intermetallic. That is, the electronic orders in APt_2X_2 intermetallics appear to emerge from an environment that includes preexisting lattice distortions and, as our density functional theory (DFT) calculations indicate, are likely to be influenced by them. Our results shed light on the genesis of CDW order in topical "112-type" intermetallics and call for more studies on the poorly known interactions between lattice distortions and emergent electronic orders in strongly correlated systems. These studies will benefit from the advanced experimental approach demonstrated here, which can be applied to any physical system exhibiting deviations from perfect crystallinity.

II. EXPERIMENT

A. Samples preparation and characterization

Polycrystalline samples of the studied intermetallics were synthesized by arc melting the constituent elements (99.99% pure, lump form) in the respective A:Pt:X molar ratios. In

*Corresponding author: petko1vg@cmich.edu

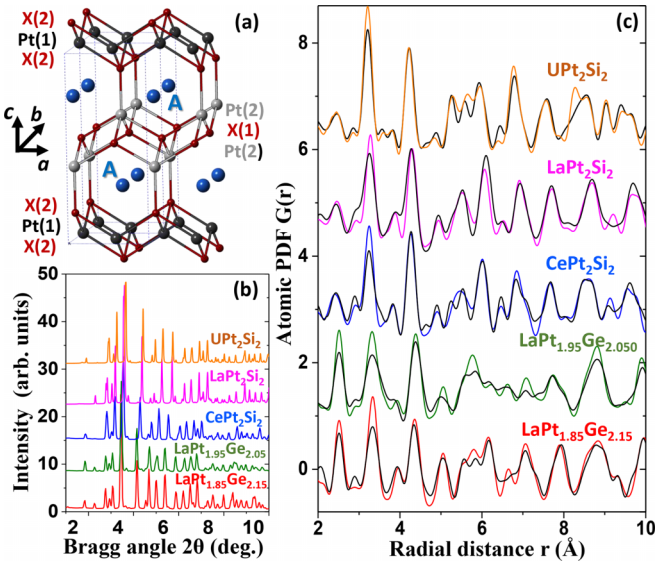

FIG. 1. (a) Crystal structure of APt_2X_2 intermetallics (A = U, La, or Ce; X = Si or Ge) featuring a sequence of alternating Pt(2)-X(1)-Pt(2) and X(2)-Pt(1)-X(2) layers and A atoms (in blue) positioned between them. Platinum atoms are in black and X atoms are brown. (b) Synchrotron XRD patterns and (c) experimental total PDFs $G(r)$ for the intermetallics, each in a different color. Experimental Pt-differential PDFs (black) are also shown in (c).

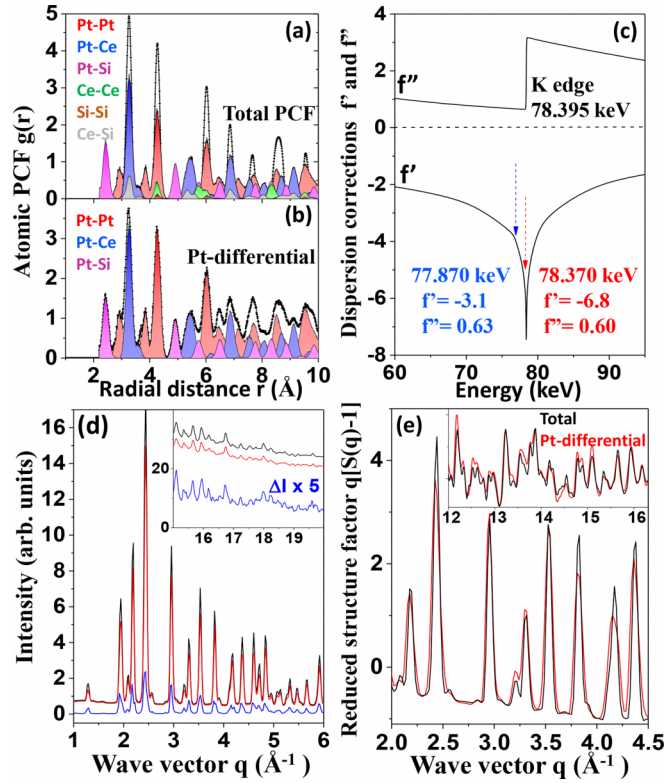

FIG. 2. Computed (a) total (black) and (b) Pt-differential atomic pair correlation functions (PCFs) $g(r)$ for $CePt_2Si_2$. The individual partial PCFs contributing to the total and Ce-differential PDFs are also shown in (a) and (b), each in a different color. (c) Energy dependence of the dispersion corrections f' and f'' to the x-ray scattering factor for Pt. The two energies below the K edge of Pt whereat XRD data were collected are marked with arrows. Values of f' and f'' for these energies are also given. (d) XRD patterns for $CePt_2Si_2$ taken at 25 eV (red) and 525 eV (black) below the K edge of Pt (78.395 keV). Their difference, ΔI (blue), is also given. (e) Experimental total (black) and Pt-differential structure factors derived from the data in (d).

line with the findings of prior studies [30–36], in-house x-ray diffraction (XRD) showed that while the as-synthesized UPt_2Si_2, $CePt_2Si_2$, $LaPt_2Si_2$, and $LaPt_{1.85}Si_{2.15}$ possess a $CaBe_2Ge_2$ type structure, space group (S.G.) $P4/nmm$, $LaPt_{1.95}Si_{2.05}$ adopts a monoclinically distorted variation of it (S.G. $P2_1/c$). This structure type [see Fig. 1(a)] features a sequence of alternating Pt(2)-X(1)-Pt(2) and X(2)-Pt(1)-X(2) layers, where Pt atoms form square planes, and the A atoms are positioned between the layers. To illustrate the emergent electronic orders, the temperature evolution of the magnetic properties of the intermetallics is shown in Supplemental Material Fig. S1 [39].

B. Synchrotron x-ray radiation experiments

Resonant total x-ray scattering experiments were conducted at beamline 1-ID-E at the Advanced Photon Source, Argonne. First, we collected data using x rays with energy of 77.870 keV (wavelength $\lambda = 0.1590$ Å), which, for reasons discussed below, is 525 eV below the K absorption edge of Pt [see Fig. 2(b)]. The samples were packed in thin Kapton tubes and scattered intensities were recorded with a single-photon-counting Pilatus3 X CdTe 2M detector, allowing us to collect high-quality data to a wave vector q_{max} of 24 Å^{-1} for less than 15 min per sample. The experimental XRD patterns are shown in Fig. 1(b). Atomic PDFs $G(r)$ derived from the patterns are shown in Fig. 1(c). They are seen to exhibit a series of well-defined peaks, each reflecting frequently occurring atomic pair distances. As such, atomic PDFs have proven sensitive to both the average crystal lattice and its distortions, including atomic displacements accompanying the formation of CDWs [40–44]. However, despite being very informative, a PDF resulting from a single diffraction experiment, usually referred to as a total PDF $G(r)$, may not necessarily clearly reveal all details in the atomic arrangement in multicomponent materials. This is because, as demonstrated in Fig. 2(a) using $CePt_2Si_2$ as an example, PDF peaks reflecting chemically distinct atomic pairs may overlap significantly, rendering their interpretation ambiguous. To resolve this problem and obtain structure data with enhanced sensitivity to the arrangement of Pt atoms, we made use of the fact that the x-ray atomic scattering factor is a function both of the wave vector and of the x-ray energy. In particular, following the protocol of resonant (anomalous) x-ray scattering [45–49] and using the same setup (Fig. S2 in [39]), we conducted a second experiment using x rays with energy of 78.370 keV ($\lambda = 0.1580$ Å), which is 25 eV below the K edge of Pt. As an example, the XRD patterns for $CePt_2Si_2$ collected at 78.370 and 77.870 keV are shown in Figs. 2(d) and S3 [39]. The intensity difference between the data sets is significant and comes entirely from differences in the atomic scattering factors of Pt atoms for the two energies, which largely arise from differences in the so-called dispersion corrections f' and f'' to the factors

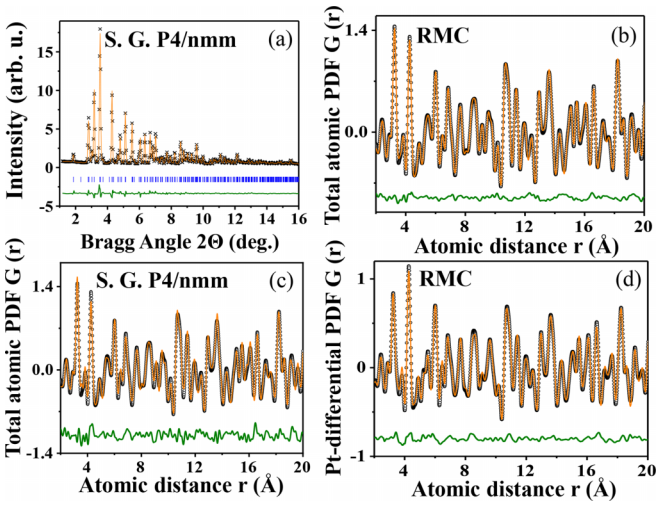

FIG. 3. Small unit cell fits (red line) to (a) XRD and (c) total PDF data (symbols) for $CePt_2Si_2$ based on a S.G. *P4/nmm* model. RMC fits (red line) to total (b) and Pt-differential (d) PDFs (symbols). The goodness-of-fit indicators R_{wp} for the small-size unit cell models in (a) and (c) are 8% and 16%, respectively. Those for the RMC fits are 5%, indicating their improved quality in comparison to the fit in (c). For clarity, the residual difference (green) is shifted by subtracting a constant. Vertical blue bars in (a) indicate Bragg peaks.

[Fig. 2(c)]. It was reduced to the so-called Pt-differential structure factor, which, when Fourier transformed, produces the so-called Pt-differential PDF. The total and Pt-differential structure factors for $CePt_2Si_2$ are compared in Fig. 2(e). The derived from them total and Pt-differential PDFs are compared in Figs. 1(c) and S4 [39]. The Pt-differential PDFs for the other four intermetallics are also shown in Fig. 1(e). As can be seen in the figures, the intensity difference between the respective total and differential Pt PDFs is significant because, contrary to the former, the latter reflect only atomic correlations involving Pt atoms, i.e., only Pt-Pt, Pt-*X*, and Pt-*A* atomic correlations, while the atomic correlations not involving Pt, i.e., *X*-*X*, *X*-*A*, and *A*-*A* correlations, which contribute to the total PDFs, are missing [Fig. 2(a)]. Thus, by using resonant total x-ray scattering, Pt-involved atomic correlations that are of a particular interest to our study were "highlighted" at the expense of the rest. More detailed descriptions of resonant total x-ray scattering can be found in Refs. [45–54]. Details of our experiment can be found in the Supplemental Material [39].

III. STRUCTURE MODELING

To assess the average crystal structure in more detail, the synchrotron XRD data were subjected to Rietveld analysis [55]. As an example, Rietveld results for $CePt_2Si_2$ are shown in Fig. 3(a). Those for the other alloys are shown in Fig. S5 [39]. The refined lattice parameters are summarized in Supplemental Material Table S2. In line with prior studies [30–36], the fits confirmed that UPt_2Si_2, $CePt_2Si_2$, $LaPt_2Si_2$, and $LaPt_{1.85}Ge_{2.15}$ exhibit a tetragonal- (S.G. *P4/nmm*) type structure, while $LaPt_{1.95}Ge_{2.05}$ is monoclinic (S.G. $P2_1/c$). No evidence for local lattice distortions was found. Then, the same models were subjected to usual PDF analysis [56]. As an example, the total PDF fit results for $CePt_2Si_2$ are shown in Fig. 3(c). Those for the other intermetallics are shown in Fig. S6 [48]. Lattice parameters that resulted from the fits are summarized in Supplemental Material Table S3 [52]. In line with the results of our recent study [42], the PDF analysis of total PDFs indicated the presence of lattice distortions in UPt_2Si_2, where the Pt(1) atoms appear displaced from their positions in the, on average, tetragonal lattice. The results for the other intermetallics were, however, inconclusive. In addition, though at an acceptable level, the quality of all fits to total PDFs appeared limited. Therefore, we carried out reverse Monte Carlo (RMC) simulations where large size models were simultaneously refined against both total and Pt-differential PDF data. The initial atomic configurations featured about 25 000-atom, 80 Å × 80 Å × 80 Å model boxes with the respective lattice symmetry. For UPt_2Si_2, $CePt_2Si_2$, $LaPt_2Si_2$, and $LaPt_{1.85}Ge_{2.15}$, the atoms in the boxes were arranged according to the rules of S.G. *P4/nmm* symmetry. For $LaPt_{1.95}Ge_{2.05}$, the atoms in the model box were arranged according to the rules of S.G. $P2_1/c$ symmetry. The large model boxes allowed us to explore lattice distortion patterns with a length scale larger than the crystallographic unit cell while maintaining the average crystallographic symmetry intact. To ensure correct stoichiometry, a respective fraction of Pt atoms in the initial $LaPt_{1.85}Ge_{2.15}$ and $LaPt_{1.95}Ge_{2.05}$ model configurations was replaced by Ge atoms, taking into account the fact that Pt and Ge positions in APt_2X_2 intermetallics are alike. This is not possible to achieve in traditional Rietveld

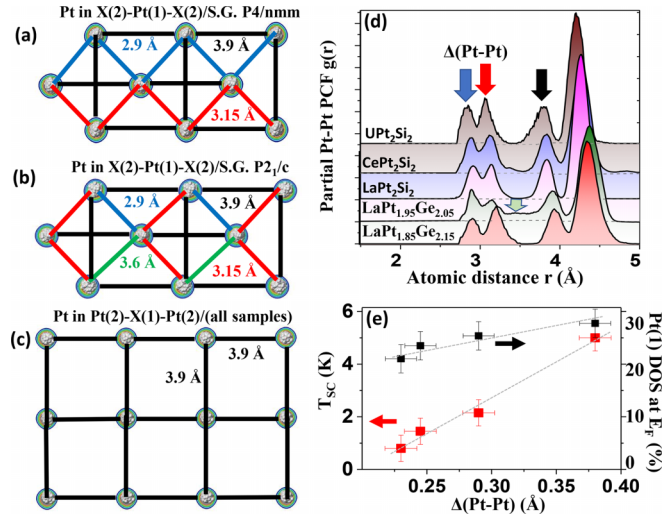

FIG. 4. Distorted Pt square plane in the (*X*)-Pt(1)-(*X*) layers in (a) UPt_2Si_2, $CePt_2Si_2$, $LaPt_2Si_2$, and $LaPt_{1.85}Ge_{2.15}$, and (b) $LaPt_{1.95}Ge_{2.05}$. The Pt square planes in the Pt(2)-*X*(1)-Pt(2) layers in all intermetallics appear undistorted, as shown in (c). Distances between Pt atoms in the planes and their values are given in different colors. The distances correspond to peaks (arrows in respective colors) in the partial Pt-Pt PCF shown in (d). The PCFs are computed from RMC refined models. (e) Temperature of the emergence of SC, T_{SC} (red symbols), and percentage contribution of Pt(1) atoms to the total DOS at E_f (black symbols) vs the difference, Δ(Pt-Pt), between near neighbor Pt-Pt distances in the distorted Pt square planes in $LaPt_{1.95}Ge_{2.05}$ (green), $LaPtSi_2$ (magenta), and $LaPt_{1.85}Ge_{2.15}$ (red). Literature data for $SrPt_2As_2$ [65,66] are also shown (black).

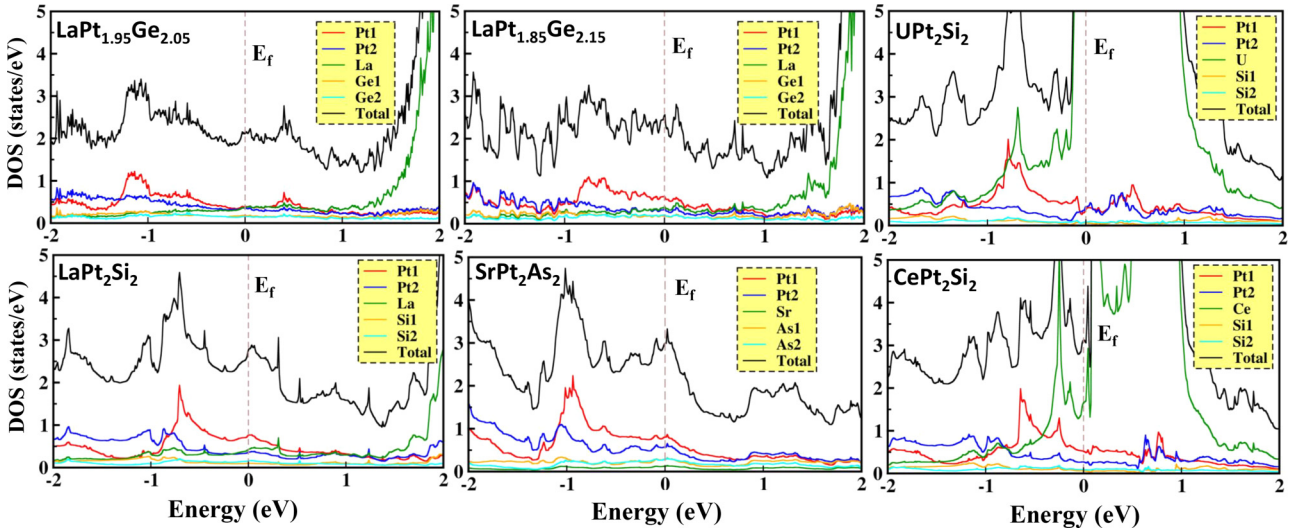

FIG. 5. Total (black) and partial (respective color) electronic density of states (DOS) for a formula unit of the studied intermetallics obtained by DFT+U calculations based on RMC refined structure models. Expanded view of the partial DOS is shown in Fig. S9 [39].

and PDF fits employing a single crystallographic unit cell. The simulations were carried out with the help of the software FULLRMC [57]. Representative RMC fits to the total and Pt-differential PDFs for $CePt_2Si_2$ are shown in Figs. 3(b) and 3(d). The RMC results for the other alloys are summarized in Figs. S7 and S8 [39]. As can be seen in the figures, the RMC simulations produce structure models that fit both the total and the Pt-differential PDFs in very fine detail. Partial Pt-Pt PDFs, reflecting the mutual arrangement of Pt atoms in the studied intermetallics, are shown in Fig. 4, as computed from the RMC refined models. Here it is to be added that, unless Pt-differential PDFs, where both the sensitivity to Pt-involving correlations is enhanced significantly (see Table S1) and Pt-involving correlations are removed, are included in the RMC modeling, the models would not converge to the results shown in Fig. 4.

IV. DISCUSSION

To understand the interaction between the lattice distortions and collective electronic orders in the studied APt_2X_2 intermetallics, we concentrate on the data in Figs. 4(a), 4(b), and 4(d). As can be seen in the figures, at room temperature, Pt atoms in the X(2)-Pt(1)-X(2) layers are already displaced from their high-symmetry positions, leading to the emergence of two first neighbor Pt-Pt distances at about 2.9 and 3.15 Å. In a hypothetical undistorted lattice, a single first neighbor Pt-Pt distance at about 3.05 Å would be observed. By contrast, Pt atoms in Pt(2)-X(1)-Pt(2) layers are not displaced from their high-symmetry position [Fig. 4(c)] and appear 3.9 Å apart. Evidently, regardless of their different chemical composition, the crystal lattice in all studied intermetallics appears unstable with respect to Pt(1) displacements at temperatures above the emergence of collectively ordered electronic states, that is, above T_{KL} in the case of UPt_2Si_2 and $CePt_2Si_2$ [36,43,58,59], and above T_{CDW} and T_{SC} in the case of La-containing intermetallics [33,60,61]. In this respect the latter appear similar to the canonical CDW system 2H-$TaSe_2$ where the periodic lattice distortions observed below T_{CDW} also emerge from well-defined local lattice distortions that exist well above T_{CDW} [62].

The magnitude of the lattice instability in the La-containing intermetallics, as measured by the difference between the spilt first neighbor Pt-Pt distances, Δ(Pt-Pt), is plotted vs T_{SC} in Fig. 4(e). Literature data for the $SrPt_2As_2$ pnictide superconductor [63–66], which adopts a $CaBe_2Ge_2$ type structure, are also shown in Fig. 4(e). As can be seen in the figure, T_{SC} scales with the magnitude of the lattice instability, indicating that the two are related. A clue about the origin of the relationship comes from DFT calculations based on the experimental structure data, as described in the Supplemental Material [39]. As can be seen in Figs. 5 and S9 [39], the density of states (DOS) at the Fermi level (E_f) in the f-electron free La- and Sr-based intermetallics appears to be dominated by the 5d electrons of Pt atoms, where the contribution of the Pt(1) atoms forming distorted square planes is larger than that of the Pt(2) atoms forming undistorted square planes. Moreover, it scales with Δ(Pt-Pt) [see Fig. 4(e)]. This result suggests that carrier conduction mainly occurs in Pt planes, where, as discussed in Ref. [65], the distorted planes would be more susceptible to emergent SC order in comparison to the undistorted ones. Then, it is tempting to speculate that, most likely due to gap-edge singularities with diverging DOS near the boundary between the ungapped and partially gapped regions of the Fermi surface emerging below T_{CDW} [24,63,64,67–69], lattice instabilities involving Pt atoms would not only give rise to periodic lattice distortions below T_{CDW} but also contribute to the emergence of SC order in the La-containing alloys. This model view is consistent with the recently put forward concept of "intertwined SC and CDW orders," where the same features of the microscopic physics, in particular local lattice distortions, produce multiple ordering tendencies with similar energy and temperature scales [70]. This far-reaching concept deserves further investigations. Interestingly, for all intermetallics studied here, Δ(Pt-Pt) also appears to scale with the atomic volume, that is, a larger

atomic volume appears to harbor larger lattice instabilities (Fig. S10). Then, it may be contemplated that, in the search for APt_2X_2 SCs with increased T_{SC}, it would be worth systematically increasing the atomic volume and, hence, the distortion in $X(2)$-Pt(1)-$X(2)$ planes beyond the values shown in Fig. 4(e) through, e.g., appropriate chemical substitution.

On the other hand, DOS at E_f in $CePt_2Si_2$ and UPt_2Si_2 appears dominated by the $4f$ and $5f$ electrons of Ce and U atoms, respectively. Not surprisingly, both alloys are heavy fermion systems. Nevertheless, at least in the case of UPt_2Si_2, the periodic distortion of Pt(1) planes emerging below T_{CDW} is found to modulate both the electronic properties and the AFM order [43,71], indicating that, in these systems, lattice distortions involving Pt atoms and electronic orders are also intertwined.

V. CONCLUSION

Efforts to understand the interaction between collective electronic states and the crystal structure, including local lattice distortions, benefit from the development of improved experimental techniques. Recent developments in synchrotron instrumentation greatly facilitate resonant total x-ray scattering experiments, opening the door to a wide use of the technique. It combines the advantages of extended x-ray absorption fine-structure spectroscopy in terms of chemical specificity and total x-ray scattering in terms of the ability to assess both short- and long-range interatomic correlations, providing an element-specific view of the crystal structure with subangstrom resolution. When combined with structure modeling, it allows one to reveal lattice distortions that would remain "hidden" in XRD patterns and total PDFs. In addition, it provides a firm structural basis for electronic properties calculations.

By applying the technique, we find that the crystal lattice of APt_2X_2 intermetallics is locally unstable with respect to distortions in one of Pt planes, leading to the presence of two first neighbor Pt-Pt distances at room temperature that locally break the crystal symmetry. The distortions scale with the atomic volume and, as found by DFT calculations, impact the DOS at E_f significantly. Thus, they would couple with collective electronic states whose emergence involves a reconstruction of the Fermi surface and eventually affect them, and vice versa. This picture may be pertinent to many strongly correlated physical systems where the lattice degrees of freedom include prominent local lattice distortions leading to CDW-like modulation of the electronic properties, rendering element-specific PDFs a convenient local structure probe to study both [79].

ACKNOWLEDGMENTS

This work was supported by the U.S. Department of Energy, Office of Science, Office of Basic Energy Sciences under Award DE-SC0021973. It also used resources of the Advanced Photon Source at the Argonne National Laboratory provided by the DOE Office of Science under Contract No. DE-AC02-06CH11357. Thanks are due to R. Amin for help with the synchrotron experiments. A portion of this work was performed at the National High Magnetic Field Laboratory, which is supported by National Science Foundation Cooperative Agreement No. DMR-2128556 and the State of Florida.

[1] J.-H. Chu, H.-H. Kuo, J. G. Analytis, and I. R. Fisher, Divergent nematic instability in an iron arsenide superconductor, Science **337**, 710 (2015).

[2] B. Keimer, S. A. Kivelson, M. R. Norman, S. Uchida, and J. Zaanen, From quantum matter to high-temperature superconductivity in copper oxides, Nature (London) **518**, 179 (2015).

[3] T. Gruner, D. Jang, Z. Huesges, R. C. Gil, G. H. Fecher, M. M. Koza, O. Stockert, A. P. Mackenzie, M. Brando, and C. Geibel, Charge density wave quantum critical point with strong enhancement of superconductivity, Nat. Phys. **13**, 967 (2017).

[4] M. Rotter, M. Tegel, and D. Johrendt, Superconductivity at 38 K in the iron arsenide $(Ba_{1-x}K_x)Fe_2As_2$, Phys. Rev. Lett. **101**, 107006 (2008).

[5] E. H. da Silva Neto, P. Aynajian, A. Frano, R. Comin, E. Schierle, E. Weschke, A. Gyenis, J. Wen, J. Schneeloch, Z. Xu, S. Ono, G. Gu, M. L. Tacon, and A. Yazdani, Ubiquitous interplay between charge ordering and high-temperature superconductivity in cuprates, Science **343**, 393 (2014).

[6] T. Rice and G. K. Scott, New mechanism for a charge density wave instability, Phys. Rev. Lett. **35**, 120 (1975).

[7] C. Phleiderer, Superconducting phases of f-electron compounds, Rev. Mod. Phys. **81**, 1551 (2009).

[8] S. Doniach, The Kondo lattice and weak antiferromagnetism, Physica B+C (Amsterdam) **91**, 231 (1977).

[9] R. Movshovich, T. Graf, D. Mandrus, J. D. Thomson, J. L. Smith, and Z. Fisk, Superconductivity in heavy fermion $CeRh_2Si_2$, Phys Rev. B **53**, 8241 (1996).

[10] G. Bulk and W. Nolting, Antiferromagnetism in $4f$ systems with lattice instabilities, Z. Phys. B **70**, 473 (1988).

[11] K. K. Kolincio, M. Roman, M. J. Winiarski, J. Strychalska-Nowak, and T. Klimczuk, Magnetism and charge density waves in $RNiC_2$ (R = Ce, Pr, and Ni), Phys. Rev. B **95**, 235156 (2017).

[12] X. Teng, L. Chen, F. Ye, E. Rosenberg, Z. Liu, J.-X. Yin, Y.-X. Jiang, J. Seop Oh, M. Zahid Hasan, K. J. Neubauer, B. Gao, Y. Xie, M. Hashimoto, D. Lu, Ch. Jozwiak, A. Bostwick, E. Rotenberg, R. J. Birgeneau, J.-H. Chu, M. Yi, and P. Da, Discovery of charge density wave in a kagome lattice antiferromagnet, Nature (London) **609**, 490 (2022).

[13] N. N. Wang, K. Y. Chen, Q. W. Yin, Y. N. N. Ma, B. Y. Pan, X. Yang, X. Y. Ji, S. L. Wu, P. F. Shan, S. X. Xu, Z. J. Tu, C. S. Gong, G. T. Liu, G. Li, Y. Uwatoko, X. L. Dong, H. C. Lei, J. P. Sun, and J.-G. Cheng, Competition between charge-density-wave and superconductivity in the kagome metal RbV_3Sb_5, Phys. Rev. Res. **3**, 043018 (2021).

[14] J. Chang, E. Blackburn, A. T. Holmes, N. B. Christensen, J. Larsen, J. Mesot, R. Liang, D. A. Bonn, W. N. Hardy, A. Watenphul, M. v. Zimmermann, E. M. Forgan, and S. M. Hayden, Direct observation of competition between

superconductivity and charge density wave order in $YBa_2Cu_3O_{6.67}$, Nat. Phys. **8**, 871 (2012).

[15] I. Hase, T. Yanagisawa, and K. Kawashima, The competition between the CDW and the superconducting state in valence skip compounds, Commun. Comput. Phys. **23**, 773 (2018).

[16] C. Peng, Y. Wang, J. Wen, Y. S. Lee, T. P. Devereaux, and H.-C. Jiang, Enhanced superconductivity by near-neighbor attraction in the doped extended Hubbard model, Phys. Rev. B **107**, L201102 (2023).

[17] C. F. Miclea, H. D. Hochheimer, B. Martin, C. Miclea, and T. Ohtani, Superconductivity and charge density wave formation in $Tl_xV_6S_8$, New J. Phys. **15**, 083008 (2013).

[18] L. F. Shi, Z. Y. Liu, J. Li, X. X. Zhang, N. N. Wang, Q. Cui, K. Y. Chen, Q. Y. Liu, P. T. Yang, J. P. Sun, B. S. Wang, Y. Uwatoko, Y. Sui, H. X. Yang, and J.-G. Cheng, Pressure-driven superconducting dome in the vicinity of CDW in the pyrite-type superconductor CuS_2, Phys. Rev. Mater. **6**, 014802 (2022).

[19] K. Cho, M. Kończykowski, S. Teknowijoyo, M. A. Tanatar, J. Guss, P. B. Gartin, J. M. Wilde, A. Kreyssig, R. J. McQueeney, A. I. Goldman, V. Mishra, P. J. Hirschfeld, and R. Prozorov, Using controlled disorder to probe the interplay between charge order and superconductivity in $NbSe_2$ Nat. Commun. **9**, 2796 (2018).

[20] W. D. Wise, M. C. Boyer, K. Chatterjee, T. Kondo, T. Takeuchi, H. Ikuta, Y. Wang, and E. W. Hudson, Charge-density-wave origin of cuprate checkerboard visualized by scanning tunnelling microscopy, Nat. Phys. **4**, 696 (2008).

[21] Y. Nagano, N. Araoka, A. Mitsuda, H. Yayama, H. Wada, M. Ichihara, M. Isobe, and Y. Ueda, Charge density wave and superconductivity of RPt_2Si_2 (R = Y, La, Nd, and Lu), J. Phys. Soc. Jpn. **82**, 064715 (2013).

[22] M. Imai, S. Ibuka, N. N. Kikugawa, T. Terashima, S. Uji, T. Yajima, H. Kageyama, and I. Hase, Superconductivity in 122-type antimonide $BaPt_2Sb_2$, Phys. Rev. B **91**, 014513 (2015).

[23] W. Ruan, X. Li, C. Hu, Z. Hao, H. Li, P. Cai, X. Zhou, D.-H. Lee, and Y. Wang, Visualization of the periodic modulation of Cooper pairing in a cuprate superconductor, Nat. Phys. Lett. **14**, 1178 (2018).

[24] K. Machida and M. Kato, Superconductivity transition temperature enhancement due to Peierls instability, Phys. Rev. B **36**, 854 (1987).

[25] Z. Du, H. Li, G. Gu, A. N. Pasupathy, J. M. Tranquada, and K. Fujita, Periodic atomic displacements and visualization of the electron-lattice interaction in the cuprate, Phys. Rev. X **13**, 021025 (2023).

[26] T. Ekino, A. M. Gabovich, M. S. Li, M. Pekała, H. Szymczak, and A. I. Voitenko, d-wave superconductivity and s-wave charge density waves: Coexistence between order parameters of different origin and symmetry, Symmetry **3**, 699 (2011).

[27] Y. Kvashnin, D. VanGennep, M. Mito, S. A. Medvedev, R. Thiyagarajan, O. Karis, A. N. Vasiliev, O. Eriksson, and M. Abdel-Hafiez, Coexistence of superconductivity and charge density waves in tantalum disulfide: Experiment and theory, Phys. Rev. Lett. **125**, 186401 (2020).

[28] C. Candolfi, M. Míšek, P. Gougeon, R. Al Rahal Al Orabi, P. Gall, R. Gautier, S. Migot, J. Ghanbaja, J. Kaštil, P. Levinský, J. Hejtmánek, A. Dauscher, B. Malaman, and B. Lenoir, Coexistence of a charge density wave and superconductivity in the cluster compound $K_2Mo_{15}Se_{19}$, Phys. Rev. B **101**, 134521 (2020).

[29] C. Y. Guo, W. B. Jiang, M. Smidman, F. Han, C. D. Malliakas, B. Shen, Y. F. Wang, Y. Chen, X. Lu, M. G. Kanatzidis, and H. Q. Yuan, Superconductivity and multiple pressure-induced phases in $BaPt_2As_2$, Phys. Rev. B **94**, 184506 (2016).

[30] Y. Lai, J. Y. Chan, and R. E. Baumbach, Electronic landscape of the f-electron intermetallics with the $ThCr_2Si_2$ structure, Sci. Adv. **8**, eabp8264 (2022).

[31] R. Gupta, A. Thamizhavel, K. P. Rajeev, and Z. Hossain, A brief review of the physical properties of charge density wave superconductor $LaPt_2Si_2$, Supercond. Sci. Technol. **35**, 084006 (2022).

[32] A. Imre, A. Hellmann, and A. Mewis, $LaPt_2Ge_2$ und $EuPt_2Ge_2$–Neubestimmung der Kristallstrukturen, Z. Anorg. Allg. Chem. **632**, 2217 (2006).

[33] S. Maeda, K. Matano, R. Yatagai, T. Oguchi, and Guo-quing Zheng, Superconductivity and the electronic phase diagram of $LaPt_{2-x}Ge_{2+x}$, Phys. Rev. B **91**, 174516 (2015).

[34] J. Lee, K. Prokes, S. Park, I. Zaliznyak, S. Dissanayake, M. Matsuda, M. Frontzek, S. Stoupin, G. L. Chappell, R. E. Baumbach, C. Park, J. A. Mydosh, G. E. Granroth, and J. P. C. Ruff, Charge density wave with anomalous temperature dependence in UPt_2Si_2, Phys. Rev. B **102**, 041112 (2020).

[35] S. Süllow, A. Otop, A. Loose, J. Klenke, O. Prokhnenko, R. Feyerherm, R. W. A. Hendrikx, J. A. Mydosh, and H. Amitsuka, Electronic localization and two-dimensional metallic state in UPt_2Si_2, J. Phys. Soc. Jpn. **77**, 024708 (2008).

[36] A. Dommann, F. Hulliger, H. R. Ott, and V. Gramlich, The crystal structure and some properties of $CePt_2Si_2$ and $CePt_2Ge_2$, J. Less-Common Met. **110**, 331 (1985).

[37] R. Hoffmann and Ch. Zheng, Making and breaking bonds in the solid state: The $ThCr_2Si_2$ structure, J. Phys. Chem. **89**, 4175 (1985).

[38] M. Shatruk, $ThCr_2Si_2$ structure type: The "perovskite" of intermetallics, J. Solid State Chem. **272**, 189 (2019).

[39] See Supplemental Material at http://link.aps.org/supplemental/10.1103/PhysRevB.108.224110 for includes details of the x-ray diffraction experiment, density functional calculations and results from fits to experimental pair distribution functions, which also contains Refs. [34,72–79].

[40] R. A. Steeman, E. Frikkee, S. A. M. Mentink, A. A. Menovsky, G. J. Nieuwenhuys, and J. A. Mydosh, Hybridisation effects in UPt_2Si_2, J. Phys.: Condens. Matter **2**, 4059 (1990).

[41] H. J. Kim, C. D. Malliakas, A. T. Tomic, S. H. Tessmer, M. G. Kanatzidis, and S. J. L. Billinge, Local atomic structure and discommensurations in the charge density wave of $CeTe_3$, Phys. Rev. Lett. **96**, 226401 (2006).

[42] V. Petkov, J. E. Peralta, B. Aoun, and Y. Ren, Atomic structure and Mott nature of the insulating charge density wave phase of 1*T*-TaS_2, J. Phys.: Condens. Matter **34**, 345401 (2022).

[43] V. Petkov, R. Baumbach, A. M. Milinda Abeykoon, and J. A. Mydosh, 3D charge density wave in the dual fermion system UPt_2Si_2, Phys. Rev. B **107**, 245101 (2023).

[44] E. S. Bozin, A. S. Masadeh, Y. S. Hor, J. F. Mitchell, and S. J. L. Billinge, Detailed mapping of the local Ir^{4+} dimers through the metal-insulator transitions of $CuIr_2S_4$ thiospinel by x-ray atomic pair distribution function measurements, Phys. Rev. Lett. **106**, 045501 (2011).

[45] Y. Waseda, *Novel Applications of Anomalous (Resonance) X-Ray Scattering for Characterization of Disordered Materials* (Springer, Berlin, 1984).

[46] N. J. Shevchik, Frequency modulated X-ray diffraction I. Determination of partial structure factors, Philos. Mag. **35**, 805 (1977).

[47] R. Serimaa, O. Serimaa, and A. Bienenstock, An improved regularization technique for the analysis of anomalous scattering data, J. Non-Cryst. Solids **192**, 372 (1995).

[48] V. Petkov, S. Shastri, J.-W. Kim, Sh. Shan, J. Luo, J. Wu, and C.-J. Zhong, Application of differential resonant high-energy X-ray diffraction to three-dimensional structure studies of nano-sized materials: A case study of Pt–Pd nanoalloy catalysts, Acta Cryst. A **74**, 553 (2018).

[49] C. T. Chantler, Theoretical form factor, attenuation, and scattering tabulation for $Z = 1 - 92$ from $E = 1 - 10$eV to $E = 0.4-1.0$ MeV, J. Phys. Chem. Ref. Data **24**, 71 (1995).

[50] A. Förster, S. Brandstetter, and C. Schulze-Briese, Transforming X-ray detection with hybrid photon counting detectors, Philos. Trans. R. Soc. A **377**, 20180241 (2019).

[51] P. K. Klug and E. L. Alexander, *X-Ray Diffraction Procedures: For Polycrystalline and Amorphous Materials* (John Wiley and Sons, New York, 1974).

[52] T. Egami and S. J. L. Billinge, *Underneath the Bragg Peaks: Structural Analysis of Complex Materials* (Pergamon Press, New York, 2003).

[53] E. Matsubara, T. Tamura, Y. Waseda, T. Zhang, A. Inoue, and T. Masumoto, An anomalous X-ray structural study of an amorphous $La_{55}Al_{25}Ni_{20}$ alloy with a wide supercooled liquid region, J. Non-Cryst. Solids **150**, 380 (1992).

[54] K. Sugiyama, A. H. Shinohara, Y. Waseda, and A. Inoue, J. Non-Cryst. Solids **192–193**, 376 (1995).

[55] J. Rodriguez-Carvajal, Recent advances in magnetic structure determination by neutron powder diffraction, Phys. B (Amsterdam, Neth.) **192**, 55 (1993).

[56] C. L. Farrow, P. Juhás, J. W. Liu, D. Bryndin, E. S. Božin, J. Bloch, Th. Proffen, and S. J. L. Billinge, PDF-fit2 and PDFgui: Computer programs for studying nanostructure in crystals, J. Phys.: Condens. Matter **19**, 335219 (2007).

[57] B. Aoun, Stochastic atomic modeling and optimization with Fullrmc, J. Appl. Cryst. **55**, 1664 (2022).

[58] R. Marcolais, C. Ayache, E. Bonjour, R. Calemczuk, M. Couach, M. Locatelli, B. Salce, D. Gignoux, D. SChmitt, and M. Zerguine, Anisotropic properties of $CePt_2Si_2$, Jpn. J. Appl. Phys. **26**, 2101 (1987).

[59] P. Dalmas de Reotier, A. Yaouanc, R. Calemczuk, A. D. Huxley, C. Marcenat, P. Bonville, P. Lejay, P. C. M. Gubbens, and A. M. Mulders, $CePt_2Si_2$: A Kondo lattice compound with no magnetic ordering down to 0.06 K, Phys. Rev. B **55**, 2737 (1997).

[60] R. Gupta, S. K. Dhar, A. Thamizhavel, K. P. Rajeev, and Z. Hossain, Superconducting and charge density wave transition in single crystalline $LaPt_2Si_2$, J. Phys.: Condens. Matter **29**, 255601 (2017).

[61] M. Falkowski, P. Doležal, A. V. Andreev, E. Duverger-Nédellec, and L. Havela, Structural, thermodynamic, thermal, and electron transport properties of single-crystalline $LaPt_2Si_2$, Phys. Rev. B. **100**, 064103 (2019).

[62] V. Petkov, K. Chapagain, S. Shastri, and Y. Ren, Genesis of the periodic lattice distortions in the charge density wave state of 2*H*-$TaSe_2$, Phys. Rev. B **101**, 121114(R) (2020).

[63] K. Kudo, Y. Nishikubo, and M. Nohara, Coexistence of superconductivity and charge density wave in $SrPt_2As_2$, J. Phys. Soc. Jpn. **79**, 123710 (2010).

[64] I. A. Nekrasov and M. V. Sadovskii, Electronic structure of novel multiple-band superconductor $SrPt_2As_2$, JETP Lett. **92**, 751 (2010).

[65] S. Kim, K. Kim, and B. I. Min, The mechanism of charge density wave in Pt-based layered superconductors: $SrPt_2As_2$ and $LaPt_2Si_2$, Sci. Rep. **5**, 15052 (2015).

[66] A. Imre, A. Hellman, G. Wenski, J. Graf, D. Johrendt, and A. Mewis, Modulated crystal structures and phase transitions—The compounds $SrPt_2As_2$ and $EuPt_2As_2$, Z. Anorg. Allg. Chem. **633**, 2037 (2007).

[67] A. Chikina, A. Fedorov, D. Bhoi, V. Voroshnin, E. Haubold, Y. Kushnirenko, K. H. Kim, and S. Borisenko, Turning charge-density waves into Cooper pairs, npj Quantum Mater. **5**, 22 (2020).

[68] A. M. Gabovich and A. I. Voitenko, Coexistence of superconductivity and charge-density waves: Evidence from tunneling studies, Low Temp. Phys. **49**, 881 (2023).

[69] A. M. Gabovich, A. I. Voitenko, T. Ekino, M. S. Li, H. Szymczak, and M. Pekała, Competition of superconductivity and charge density waves in cuprates: Recent evidence and interpretation, Adv. Condens. Matter Phys. **10**, 681070 (2010).

[70] A. Fang, A. G. Singh, J. A. W. Straquadine, I. R. Fisher, S. A. Kivelson, and A. Kapitulnik, Robust superconductivity intertwined with charge density wave and disorder in Pd-intercalated $ErTe_3$, Phys. Rev. Res. **2**, 043221 (2020).

[71] F. Kon, C. Tabata, K. Miura, R. Hibino, H. Hidaka, T. Yanagisawa, H. Nakao, and H. Amitsuka, Correlation between antiferromagnetic and charge-density-wave order in UPt_2Si_2 studied by resonant x-ray scattering, SciPost Phys. Proc. **11**, 011 (2023).

[72] V. Petkov, Nanostructure by high-energy X-ray diffraction, Mater. Today **11**, 28 (2008).

[73] G. R. Munro, Reliability of partial structure factors determined by anomalous dispersion of x-rays, Phys. Rev. B **25**, 5037 (1982).

[74] A. P. Hammersley, S. O. Svensson, M. Hanfland, A. N. Fitch, and D. Häusermann, Two-dimensional detector software: From real detector to idealised image or two-theta scan, High Pressure Res. **14**, 235 (1996).

[75] V. Petkov, RAD, a program for analysis of X-ray diffraction data from amorphous materials for personal computers, J. Appl. Crystallogr. **22**, 387 (1989).

[76] J. P. Perdew, K. Burke, and M. Ernzerhof, Generalized gradient approximation made simple, Phys. Rev. Lett. **77**, 3865 (1996).

[77] G. Kresse and J. Furthmüller, Efficient iterative schemes for *ab initio* total-energy calculations using a plane-wave basis set, Phys. Rev. B **54**, 11169 (1996).

[78] H. T. Ma, X. Ming, X. J. Zheng, J. F. Wen, Y. C. Wang, Y. Liu, and H. Li, Node-line Dirac semimetal manipulated via Kondo mechanism in nonsymmorphic $CePt_2Si_2$, Phys. Rev. B **107**, 075124 (2023).

[79] D. J. Mukkattukavil, J. Hellsvik, A. Ghosh, E. Chatzigeorgiou, E. Nocerino, Q. Wang, K. Von Arx, S. W. Huang, V. Ekholm, Z. Hossain, and A. Thamizhavel, Resonant inelastic soft x-ray scattering on $LaPt_2Si_2$, J. Phys.: Condens. Matter **34**, 324003 (2022).